

Evolution of the cluster abundance in non-Gaussian models

James Robinson[★] and Jonathan E. Baker[†]

Department of Astronomy, University of California, Berkeley CA 94720

8 August 2018

ABSTRACT

We carry out N-body simulations of several non-Gaussian structure formation models, including Peebles' isocurvature cold dark matter model, cosmic string models, and a model with primordial voids. We compare the evolution of the cluster mass function in these simulations with that predicted by a modified version of the Press-Schechter formalism. We find that the Press-Schechter formula can accurately fit the cluster evolution over a wide range of redshifts for all of the models considered, with typical errors in the mass function of less than 25%, considerably smaller than the amount by which predictions for different models may differ. This work demonstrates that the Press-Schechter formalism can be used to place strong model independent constraints on non-Gaussianity in the universe.

Key words: Cosmic strings – cosmology: theory – large-scale structure of universe – galaxies: clusters: general

1 INTRODUCTION

Many cosmological models, including ‘inflation’, predict that the large scale structure of the universe arose from the gravitational collapse of Gaussian primordial fluctuations. These models have a strong physical motivation (in inflation, the primordial perturbations are just quantum fluctuations), require few free parameters (the two-point correlation function provides a complete statistical description of the field), and have many observable properties which can be modeled with simple physics. Given these attractive features, Gaussian models are a natural starting point for the investigation of structure formation.

A number of theories however, including ‘defects’ (Kibble 1976, Vilenkin & Shellard 1994) and certain exotic forms of inflation (Peebles 1983, 1997, 1998a,b; La 1991; Amendola & Occhionero 1991; Amendola & Borgani 1993), predict that the primordial fluctuations were not Gaussian. These theories possess many of the attractive features of Gaussian models: defect models, for instance, are well motivated and require few free parameters. Unlike the Gaussian case, however, making robust predictions in non-Gaussian models is often very difficult. In defect theories, this is because the physical processes which must be modeled are complex and highly non-linear. More generally, the parameter space available to non-Gaussian models is infinitely larger, because specifying the statistics of the primordial fluctuations re-

quires not just the two-point correlation function, but all higher n -point correlation functions as well.

Previous studies of non-Gaussian structure formation (e.g., Weinberg & Cole 1992; Borgani et al. 1994; Park, Spergel & Turok 1991) have tended to concentrate on specific models, making predictions for observable properties in each case. Due to the infinite range of possible parameters, and the difficulties of making robust predictions even within well specified models, we turn here to a different approach: We start from a property of non-Gaussian models which can be fully quantified by a small number of parameters, the probability distribution function (PDF) of the density field over the range of scales relevant to galaxy cluster formation. While knowledge of the PDF does not fully specify the non-Gaussian nature of the distribution (which would require knowledge of all the higher n -point correlation functions), we show that it provides us with sufficient information to make robust predictions for a very interesting observable quantity: the redshift evolution of the cluster number abundance. We do this by demonstrating that the cluster evolution in non-Gaussian N-body simulations can be accurately described by a version of the Press-Schechter formalism (Press & Schechter 1974) modified to allow for non-Gaussianity (Chiu, Ostriker & Strauss 1997), which requires only the PDF as input. The result of this work is a powerful tool with which we can use observations of galaxy clusters to constrain the primordial PDF in the universe, without reference to any specific non-Gaussian models or the uncertainties which may be inherent to them. The work presented here validates a number of previous studies which have used the non-Gaussian Press-Schechter formalism, but

[★] jhr@palan.berkeley.edu

[†] jbaker@draco.berkeley.edu

have not tested it (Chiu et al. 1998, Robinson, Gawiser & Silk 1998, van de Bruck 1998). Other work (Robinson, Gawiser & Silk in preparation) discusses in detail the strong model-independent constraints we can place using this tool.

In §2 we describe the PS formalism, and we extend the derivation in the non-Gaussian case to allow for a scale dependent probability distribution function. Section 3 describes our non-Gaussian models and the realization of the initial density fields in each case. In §4 we give details of our N-body simulations. Finally, in §5 we present our results and in §6 we discuss our conclusions.

2 MODIFIED PRESS-SCHECHTER FORMALISM

The Press-Schechter (PS) formalism (Press & Schechter 1974) is a simple semi-analytic tool for predicting the expected number density of clusters in an evolved density field, given the linear initial conditions. Extensive work has shown that this formalism can give a good fit to the cluster abundance observed in N-body simulations of Gaussian structure formation models. Though the PS formula has mainly been applied to Gaussian fluctuations, there is a straightforward way to generalize it to the non-Gaussian case: Here, the statistics of the underlying density field are quantified by specifying its PDF $p_R(\delta)$, where $p_R(\delta) d\delta$ is the probability that the primordial field at a given point in space has an overdensity between δ and $\delta + d\delta$ after a top hat smoothing of scale R . We can rewrite $p_R(\delta)$ in terms of a rescaled PDF $P_R(y)$ which has zero mean and *rms* one: $p_R(\delta) = P_R(\delta/\sigma_R)/\sigma_R$, where σ_R is the *rms* overdensity in spheres of radius R . For many non-Gaussian models it should be a reasonable assumption that only the *rms* value of δ varies as a function of scale (for instance, in defect theories where the fluctuations are laid down in a scale invariant manner), so that $P_R(y)$ is in fact independent of R . The Press-Schechter formula for this case has been derived by Chiu et al. (1998) and used to make predictions for a number of non-Gaussian scenarios (Robinson et al. 1998; van de Bruck 1998).

In this work, we rederive the formula for the more general case that the form of the PDF does depend on scale, since we will see later that the assumption of scale independence is valid for some but not all of the models we consider. The Press-Schechter formalism starts from the assumption that clusters with mass greater than some value M at redshift z form in regions of the primordial density field whose overdensity smoothed on scale R_M and extrapolated using linear gravity to redshift z is greater than some critical value δ_c . The scale R_M is chosen to be the radius of a sphere containing mass M in the primordial homogeneous universe, which satisfies

$$M = \frac{4\pi}{3} \rho_m R_M^3, \quad (1)$$

where ρ_m is the comoving matter density of the universe. The critical threshold δ_c is taken from an analytic solution for the collapse of a spherically symmetric overdensity, which gives $\delta_c = 1.69$ for a critical universe (for a derivation of the weak cosmological dependence, see Lacey & Cole 1993, Eke et al. 1996).

From this starting point, it is possible to derive the

cluster mass function. The probability $\mathcal{P}_{>R}$ of a point in space forming part of a cluster with Lagrangian radius larger than R is equal to the probability of the density field, after smoothing on scale R , having an overdensity larger than the critical overdensity δ_c . That is,

$$\mathcal{P}_{>R} = \int_{\delta_c}^{\infty} p_R(\delta) d\delta. \quad (2)$$

To obtain the probability $\mathcal{P}_R dR$ of a point in space forming part of a cluster with Lagrangian radius between R and $R + dR$, we differentiate the above expression with respect to R and take the absolute value,

$$\mathcal{P}_R dR = \left| \frac{d}{dR} \mathcal{P}_{>R} \right| dR. \quad (3)$$

We can obtain the number density of such clusters $n(R) dR$ by dividing by the cluster Lagrangian volume,

$$n(R) dR = \frac{3f}{4\pi R^3} \left| \frac{d}{dR} \mathcal{P}_{>R} \right| dR, \quad (4)$$

where we have also multiplied by a correction factor f , whose value we will fix by ensuring that final mass function accounts for the entire mass of the universe. The integrated mass function $N_{>M}$ is then given by

$$N_{>M} = \frac{3f}{4\pi} \int_{R_M}^{\infty} \frac{dR}{R^3} \left| \frac{d}{dR} \mathcal{P}_{>R} \right|. \quad (5)$$

To fix the value of the correction factor f , we use the following expression for the integrated mass density ρ_m of the universe:

$$\rho_m = \int_0^{\infty} M_R n(R) dR, \quad (6)$$

where M_R is the cluster mass corresponding to Lagrangian radius R . Substituting using equation 1 and 4, we find

$$f = (\mathcal{P}_{>R}|_{R=0})^{-1} \quad (7)$$

which does indeed give $f = 2$ for Gaussian fluctuations, as originally proposed by Press & Schechter.

We comment briefly on some computational issues: We can rewrite the mass function in a convenient form using integration by parts,

$$N_{>M} = \frac{3f}{4\pi} \left| \frac{1}{R_M^3} \mathcal{P}_{>R_M} - 3 \int_{R_M}^{\infty} \frac{dR}{R^4} \mathcal{P}_{>R} \right|. \quad (8)$$

For each model and for each redshift we compute and store the function $\mathcal{P}_{>R}$ for a range of values of R . Each computation of $N_{>M}$ (eq. 8) then requires only a single integration over these stored values. Finally, we note that the redshift dependence of the mass function arises through the dependence of $\mathcal{P}_{>R}$ on redshift, which for conciseness we have not labelled explicitly here.

3 NON-GAUSSIAN MODELS

For the purposes of this work, we consider three classes of non-Gaussian model; Peebles' isocurvature cold dark matter (ICDM) model, cosmic string models, and primordial void models. These models are all physically motivated, and each one represents an interesting structure formation scenario in its own right. However, each model has a number

of uncertain features. In the cases of ICDM or Voids, there is a wide range of possible model parameters to consider, and in the case of cosmic strings, there are extreme computational difficulties involved in realistically evolving a string network. Here we will not be concerned with these uncertainties, since our goal is simply to pick a diverse set of concrete non-Gaussian models, and use these examples to test the applicability of the non-Gaussian PS formalism. To the extent to which the formalism works, we will have a tool with which we can make specific predictions for cluster evolution in a wide class of non-Gaussian models, taking as input only the initial PDF $p_R(\delta)$ (which is what enters into the PS calculation; see §2). We will then be able to use cluster evolution to constrain the initial PDF of the universe without referring to any specific non-Gaussian models, a possibility which will be extremely useful given the difficulty of making robust predictions in so many non-Gaussian scenarios.

We now explain the motivation for each of the models, and present the computational details of realizing initial density fields in each case.

3.1 Peebles ICDM model

The first non-Gaussian structure formation scenario we consider is the Peebles ICDM model (Peebles 1983, 1997, 1998a,b). This is an inflationary model which gives rise to non-Gaussian isocurvature fluctuations in the matter distribution. The cold dark matter (CDM) in this model is a field $\phi(\mathbf{x})$ with mass density

$$\rho(\mathbf{x}) \propto \phi(\mathbf{x})^2 \quad (9)$$

which survives as a relic at the end of inflation. Perturbations in this CDM field grow from quantum fluctuations which are frozen during the accelerated expansion of the universe. The perturbations in $\phi(\mathbf{x})$ are Gaussian, with power spectrum

$$P_\phi \propto k^{m_\phi} \quad (10)$$

over a broad range of scales, where the spectral index m_ϕ depends on the details of the model. The corresponding fluctuations in ρ are non-Gaussian, and it is easy to show that they have an initial power spectrum

$$P_\rho \propto k^{m_\rho}, \quad (11)$$

with

$$m_\rho = 3 + 2m_\phi. \quad (12)$$

Due to the isocurvature nature of the fluctuations, the CDM density does not evolve until the matter era, and then only on scales which are inside the horizon. Those modes which have crossed the horizon before matter-radiation equality will all start to grow at that time, while those modes which enter the horizon later will be increasingly suppressed. For our investigation of cluster formation we are interested mainly in the former, smaller scales, so it will be sufficient to assume scale-independent linear growth of the initial fluctuations.

We consider two values of the initial spectral index of the Gaussian field m_ϕ . First, we consider a model (which we denote ICDM-2.4) with $m_\phi = -2.4$, in a background cosmology with $\Omega_m = 0.2$ and $\Omega_\Lambda = 0.8$. This set of parameters has been suggested as an interesting starting point by

Peebles (1998b) since it gives power spectra in reasonable agreement with large scale structure and CMB data. Second, we consider a model (ICDM-2.0) with $m_\phi = -2.0$, in a background cosmology with $\Omega_m = 1$ and $\Omega_\Lambda = 0$. We do not expect this model to give a particularly good fit to the large scale structure data, but we introduce it since the degree of non-Gaussianity is intermediate between that of (ICDM-2.4) and a Gaussian distribution, and it therefore allows us to test the Press-Schechter formalism over a wider range of models.

For each ICDM model, we generate a 128^3 realization of a Gaussian random field $\phi(\mathbf{x})$ with the appropriate power spectrum $P(k) \propto m_\phi$. We then compute $\rho(x) = \phi(x)^2$, and the corresponding density perturbation

$$\delta(x) = \frac{\rho(x) - \bar{\rho}}{\bar{\rho}}, \quad (13)$$

where $\bar{\rho}$ is the mean density, given by

$$\bar{\rho} = \frac{1}{N} \sum_N \rho(x), \quad (14)$$

and N is the number of points on the lattice. Finally, we rescale the density contrast so that the density field will have the correct value of σ_8 when linearly evolved to $z = 0$.

3.2 Cosmic Strings

The second class of non-Gaussian model we consider is that of cosmic strings. Here, structure is seeded gravitationally by an evolving network of string-like ‘defects’, topological relics of a symmetry breaking phase transition in the very early universe (Kibble 1976; Vilenkin & Shellard 1994). Recent work suggests that cosmic strings in a critical universe do not give a viable theory of structure formation (Allen et al 1997; Albrecht, Battye & Robinson 1997), although strings in a universe with a significant cosmological constant may be able to give a good fit to existing large scale structure data (Battye, Robinson & Albrecht 1998; Avelino et al 1998). For the purposes of this work, we shall not be concerned by the many uncertainties in the details of realistic string dynamics. Instead, we shall take a simple representative model and use it as a testing ground for our study of cluster evolution.

Our string-seeded density models use the string simulations of Ferreira (1995). These simulations evolve a network of strings in flat space, where an exact solution of the equations of motion exists (Smith & Vilenkin 1987). Although the string simulations are carried out in a flat space background, the network evolution demonstrates many of the important properties which are seen in expanding universe simulations, the most important of which is the ‘scaling’ of the string density, ensuring that the induced density perturbations will be roughly scale invariant on the largest scales.

Following Veeraraghavan & Stebbins (1990), the matter overdensity δ induced by the network can be computed by convolving a component $\theta_+ = \theta_{00} + \theta_{ii}$ of the string stress-energy with a suitable Green function, and integrating over time. That is,

$$\tilde{\delta}(\mathbf{k}) = 4\pi \int_{\eta_i}^{\eta_f} d\eta' T(\mathbf{k}, \eta') \tilde{\theta}_+(\mathbf{k}, \eta') \frac{1}{1 + (k_c/k)^2}, \quad (15)$$

where η_i and η_f are the initial and final times in the simulation, $\tilde{\delta}(\mathbf{k})$ is the Fourier transform of the induced overden-

sity, \tilde{T}_2^C is a transfer function taken from Veeraraghavan & Stebbins (1990), $\eta = \int_0^t dt/a$ is the conformal time, a is the cosmological scale factor, and the last term is a ‘compensation factor’, with compensation scale $k_c = 2\pi/\eta$, included to ensure artificially that the density evolution conserves stress energy on the largest scales.

We carry out our flat space string simulations on a 128^3 lattice, choosing the side of our box to be $100h^{-1}$ Mpc. We work out the conformal time η at each time-step by equating it to the simulation horizon size (which is zero at the initial time and grows by one lattice spacing at each time-step). At each step, we compute the appropriate component $\theta_+(\mathbf{x})$ of the string stress energy tensor on the lattice, Fourier transform to obtain $\tilde{\theta}_+(\mathbf{k})$, and multiply by $T(\mathbf{k}, \eta)$. The final density contrast is then given by the sum of individual contributions from each time-step, as in eq. 15. Since all significant perturbations are induced at a time when the fluctuations are still linear, it is sufficient to use linear gravity in this way to compute the initial density field, and only consider the effects of non-linear gravity in the subsequent evolution. We choose two representative string models. First, we consider a model with an $\Omega_m = 1$ hot dark matter (HDM) background with one species of massive neutrino accounting for the entire mass of the universe, and a Hubble constant $H_0 = 100h$ km s $^{-1}$ Mpc $^{-1}$ with $h = 0.5$. We denote this model ‘Strings-HDM’. Second we consider a string network in an $\Omega_m = 1$ CDM background, also with $h = 0.5$, which we denote ‘Strings-CDM’.

3.3 Primordial Voids

The final non-Gaussian model we consider is one where the matter distribution has an enhanced network of primordial voids. The physical motivation for such models comes from an inflationary theory with two scalar fields (La 1991): one field drives inflation, while at the same time the second field undergoes a first order phase transition. The bubbles nucleated in this phase transition give rise to under-densities in the CDM distribution, superimposed on Gaussian fluctuations which are also generated during the inflationary epoch. The detailed properties of the bubble distribution, including their sizes, shapes and profiles, will depend on the exact nature of the inflationary model, but for some range of parameters it is possible to produce bubbles which are large enough to have a significant impact on structure formation, yet still escape limits arising from current Cosmic Microwave Background (CMB) observations (Amendola & Occhionero 1991; Amendola & Borgani 1993).

A typical cosmologically interesting scenario would produce a dense network of bubbles with radii of order $10-40h^{-1}$ Mpc. For the purposes of this work, we generate a simple realization of such a model as follows: in a $100h^{-1}$ Mpc box, we generate a 128^3 realization of a Gaussian density field $\delta_g(\mathbf{x})$, with a power spectrum $P_\rho \propto k^{-1.8}$. This spectral index is chosen so that the density field has a very similar power spectrum to that in the ICDM-2.4 model, thus ensuring that our simulations primarily compare the effect of varying the amount of non-Gaussianity in the fluctuations, rather than that of varying the spectral index. We then superimpose on this a distribution of N_v randomly located voids, where the voids are spherically symmetric top-hat under-densities with radius $R = 12h^{-1}$ Mpc. The total density field is given by

$$\delta(\mathbf{x}) = \delta_g(\mathbf{x}) - \delta_V \sum_{i=1}^{N_v} W_R(\mathbf{x} - \mathbf{y}_i), \quad (16)$$

where δ_V is the amplitude of the void under-density, \mathbf{y}_i is the centre of the i^{th} void and $W_R(\mathbf{x})$ is the window function in real space of a spherical top-hat with radius R , that is:

$$W_R(\mathbf{x}) = \begin{cases} 1 & \dots |\mathbf{x}| \leq R \\ 0 & \dots \text{otherwise.} \end{cases} \quad (17)$$

We dial the amplitude of the void under-density δ_V to ensure that the resulting matter field has a significant degree of non-Gaussianity, without completely swamping the Gaussian component of the distribution. We find $\delta_V = 0.1\sigma_{g,8}$ is a suitable value, where $\sigma_{g,8}$ is the *rms* value of the Gaussian component, after top-hat smoothing on a scale of $8h^{-1}$ Mpc. We choose $N_v = 12$, and generate the void centres \mathbf{y}_i by picking points at random, discarding any choices which would give rise to overlapping voids, and repeating until the number of acceptable centres equals N_v . Finally we rescale the field $\delta(\mathbf{x})$ to ensure that it has the chosen normalization σ_8 .

4 DETAILS OF N-BODY RUNS

In §3 we have explained the motivation for our non-Gaussian models, and set out in detail the processes involved in generating density fields which realize these models. We now describe the techniques involved in transforming these linear density fields into initial conditions for N-body simulations. For each of the models in question we start from a density field $\delta(\mathbf{x})$ defined on a 128^3 lattice. The N-body simulations require initial conditions in the form of positions and velocities of some number $N_p = n_p^3$ particles, which we can generate from our density fields using the Zeldovich approximation (Zeldovich 1970). Specifically, we define a displacement field $\mathbf{p}(\mathbf{q})$ via

$$\nabla \cdot \mathbf{p}(\mathbf{q}) = -\delta_0(\mathbf{q}), \quad (18)$$

where the subscript zero denotes the density field extrapolated to the present day assuming linear growth. Starting from a regular grid of particles, the position $\mathbf{x}(z)$ of each particle at redshift z is given by

$$\mathbf{x}(z) = \mathbf{q} + \mathbf{p}(\mathbf{q}) \frac{b(z)}{b(0)}, \quad (19)$$

where $b(z)$ is the linear growth factor at redshift z , and q is the initial coordinate of the particle. The comoving velocity of that particle is given by

$$\mathbf{v}(\mathbf{q}, z) = \mathbf{p}(\mathbf{q}) \frac{b(z)}{b(0)} \frac{d \ln b}{dt} \quad (20)$$

where t is the physical time. We can solve eq. 18 for the displacement field efficiently using Fourier transforms, that is:

$$\tilde{\mathbf{p}}(\mathbf{k}) = \mathbf{G}(\mathbf{k}) W(\mathbf{k}) \tilde{\delta}(\mathbf{k}), \quad (21)$$

where $\tilde{\mathbf{p}}(\mathbf{k})$ is the Fourier transform of the displacement field $\mathbf{p}(\mathbf{x})$, G is the appropriate Green function,

$$\mathbf{G}(\mathbf{k}) = -i \frac{\mathbf{k}}{k^2}, \quad (22)$$

and $W(\mathbf{k}) = w(k_1)w(k_2)w(k_3)$ is a smoothing function, whose form is chosen to optimize agreement between the power spectrum of the input density field $\delta(\mathbf{x})$ and that of the mass distribution represented by the displaced particles (which we can measure by resampling the particle distribution as a new density field on a lattice). We find the choice

$$w(k) = \begin{cases} 1 & \dots kL/n_p < \pi \\ 0 & \dots \text{otherwise} \end{cases} \quad (23)$$

gives good agreement.

We evolve each density field using P^3M simulations carried out on a GRAPE-3AF board attached to a Sun workstation. The GRAPE-3AF is a special purpose computer which quickly evaluates pairwise forces, allowing a cosmological simulation with 64^3 particles to be run in under a day. The code used for our simulations is based on the P3MG3A algorithm described by Brieu, Summers, & Ostriker (1995).

Each simulation contains $N_p = n_p^3 = 64^3$ particles with a particle mass of $1.05 \times 10^{12} \Omega_m h^{-1} M_\odot$. The effective force resolution η is 0.128 times the mean inter-particle separation, or $200h^{-1}$ kpc for our $100h^{-1}$ Mpc box length. The initial redshifts z_i for each model, chosen in each case by ensuring that $\Delta^2 < 0.15$ at the Nyquist frequency, are given in Table 1. For a given amplitude of fluctuations, the criterion of no shell crossing generally forces us to adopt an earlier initial redshift in the non-Gaussian models than in the corresponding Gaussian case. Outputs from the simulations are stored and analyzed for a number of redshifts between $z = z_i$ and $z = 0$.

For each output, we identify clusters in the simulations using the ‘friends-of-friends’ (FOF) algorithm. This algorithm defines clusters as those groups of particles which are connected by pairs whose separation is smaller than some linking parameter l , which is quoted in units of the mean inter-particle separation. We choose $l = 0.2$, so that the mean overdensity within the clusters identified is of order 200. This choice of linking length has been shown to pick out clusters whose mass function is in good agreement with the PS prediction in the case of Gaussian fluctuations (Mo, Jing & White 1996).

5 RESULTS

We now compare the predictions of the modified PS formalism with the results of our simulations. In order to compute the PS prediction, we require as input for each model the amplitude of the fluctuations (quantified in terms of σ_8), the form of the power spectrum $P(k)$, and the PDF $P_R(y)$ (renormalized to have mean zero and standard deviation one) as a function of scale. For our non-Gaussian models we do not have simple analytic expressions for these quantities, so instead we must measure them directly in the simulations. To do this, we output the particle positions and velocities at an early redshift $z_1 = (z_i - 1)/2$, when all scales of interest are still in the linear regime. We compute the PDF of the field on a range of scales R by throwing down 30,000 spheres at random and counting the distribution of particle numbers in each sphere. We compute the power spectrum by resampling the particle distribution as a density field on a 128^3 lattice, and performing the appropriate Fourier transform.

With Gaussian simulations, it is not normally necessary

to carry out these steps, since, in constructing a realization of a Gaussian field it is straightforward to ensure that it has the correct normalization, power spectrum and PDF. In order to test the fairness of the techniques we are using to measure these quantities in the non-Gaussian case, we carry out an identical analysis on a simulation (which we denote $GA-1.8$) with Gaussian initial conditions and a power spectrum $P(k) \propto k^{-1.8}$, in a background cosmology with $\Omega_m = 0.2$ and $\Omega_\Lambda = 0.8$.

The power spectrum and PDF $P_R(y)$ with $R = 8h^{-1}$ Mpc (the Lagrangian radius of a typical rich cluster) of the linear initial conditions for each model are shown in Figs. 1, 2, 3, 4, 5, and 6. The solid lines show the quantities computed from the simulations, and the dotted lines show simple analytic fits that we have used as input to the PS predictions. We fit the power spectrum with a two parameter model:

$$P(k) = 10^{C_1 \log_{10} k + C_2 (\log_{10} k)^2}, \quad (24)$$

where we compute the parameters C_1 and C_2 for each model by a simple least squares fitting to all points $k < k_{Ny}$, and $k_{Ny} = \pi L/n_p$ is the Nyquist frequency of the box. The enhanced power in modes with $k > k_{Ny}$ is an artifact of the finite mass resolution of the simulations; it does not affect the subsequent evolution. For the cosmic string case, use of two parameters significantly improves the fit to the data, but for all other models we can obtain a good fit by setting $C_2 = 0$. In the $ICDM-2.4$ model, the best fit power spectrum has a slope $m_\rho = -1.6$, which should be compared with value $m_\rho = 3 + 2m_\phi = -1.8$ which we would expect from a theoretical calculation (see eq. 12). The slightly shallower slope arises from missing power on large scales, where the assumption of a pure power law in the scalar field ϕ breaks down due to finite size effects. In the $GA-1.8$ model, the best fit slope is $P(k) \propto k^{-1.82}$, very close to the theoretical value of -1.8 which we have fed in.

We fit the PDF $P_R(y)$ with a log-normal distribution, translated and normalized to have mean zero and standard deviation one, that is:

$$P_{LN}^A(y) = \frac{C}{\sqrt{2\pi A^2}} e^{-x^2(y)/2 - |A|x(y)}, \quad (25)$$

where

$$x(y) = \frac{\ln(Cy|A|/A + B)}{|A|} \quad (26)$$

with

$$B = e^{A^2/2} \quad (27)$$

$$C = \sqrt{B^4 - B^2}. \quad (28)$$

The log-normal distribution has one free parameter A , with $A > 0$ giving rise to an extended tail of positive fluctuations, $A < 1$ giving rise to a suppressed tail of positive fluctuations, and Gaussianity in the limit $A \rightarrow 0$. We fit the PDF $P_R(y)$ in each model by finding the value of A for which the number of peaks of height 3σ or greater is equal to that for $P_R(y)$, that is we solve for A satisfying

$$\int_3^\infty P_R(y) dy = \int_3^\infty P_{LN}^A(y) dy. \quad (29)$$

The log-normal PDFs fitted by this procedure also give a good fit for all values of y , as demonstrated by our figures.

Model	$P(k)$					$P_R(y)$		
	Ω_m	Ω_Λ	z_i	σ_8	C_1	C_2	A_1	A_2
GA-1.8	0.2	0.8	19	0.98	-1.82	0	0	0
ICDM-2.4	0.2	0.8	39	0.99	-1.60	0	0.58	0
ICDM-2.0	1.0	0.0	29	1.0	-0.98	0	0.35	0
Strings-HDM	1.0	0.0	19	0.58	-6.95	-3.67	0.17	0
Strings-CDM	1.0	0.0	29	0.86	-1.9	-0.6	0.19	-0.012
Voids	1.0	0.0	15	0.89	-2.07	0	0.154	-0.049
								0.001

Table 1. Summary of each of the models, including background cosmology, normalization, power spectrum and PDF parameters.

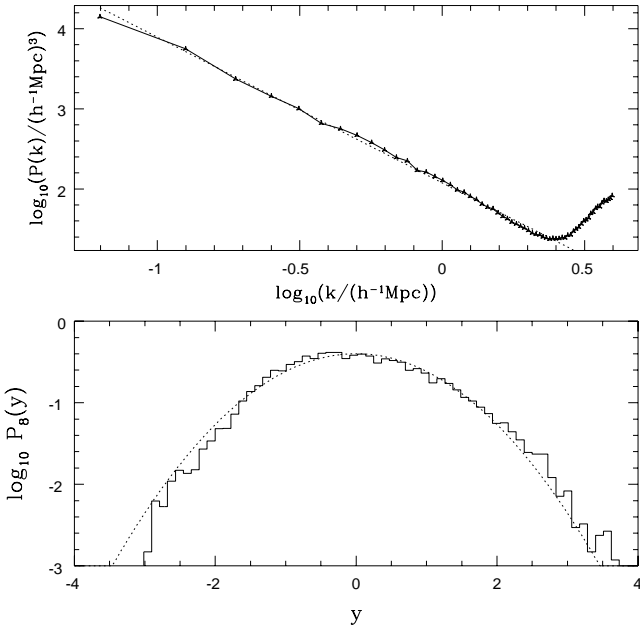


Figure 1. Measured (solid lines) and fitted (dotted lines) power spectra (top panel) and PDF (bottom panel) in the Gaussian GA-1.8 model.

We find that we can fit the scale dependence of the parameter A using a quadratic function in R , truncated to ensure that it does not change sign, that is

$$A(R) = \begin{cases} A_1 + A_2 R + A_3 R^2 & \dots \frac{A_1 + A_2 R + A_3 R^2}{(A_1 + A_2 R + A_3 R^2)_{R=8}} > 0 \\ 0 & \dots \text{otherwise.} \end{cases} \quad (30)$$

For all but the Voids model, $P_R(y)$ is very nearly scale independent over the range of scales relevant to cluster formation in our simulation, and it is sufficient to set the parameters A_2 and A_3 to zero. In the Gaussian case, we find that the best fit value of A is very slightly greater than zero, but that the predictions for $N_{>M}$ are virtually identical whether we

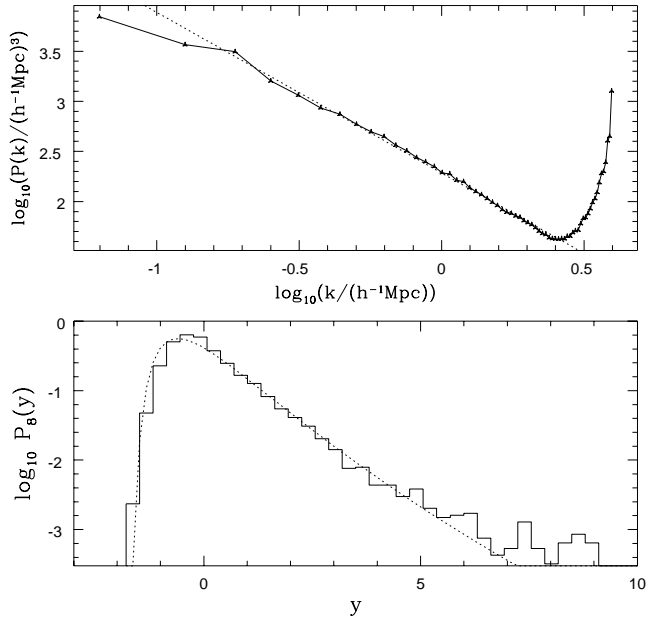


Figure 2. Measured (solid lines) and fitted (dotted lines) power spectra (top panel) and PDF (bottom panel) in the ICDM-2.4 model.

use this best fit value or the choice $A = 0$. Values for the parameters σ_8 , C_1 , C_2 , A_1 , A_2 , and A_3 used to fit the normalization, power spectrum, and PDF in each of our models are given in Table 1.

In Figs. 7, 8, 9, 10, 11, and 12 we compare the PS prediction $N_{>M}$ for the mass function (curves) with the mass function $N_{>M}^S$ measured in the simulations (data points), for a range of output times. For the simulations, we restrict our analysis to that portion of the mass function $N_{>M}^S$ for which $M > 16M_p$, where M_p is the mass of a single particle. In the Gaussian case, the PS prediction typically gives a good fit to the mass function observed in simulations for

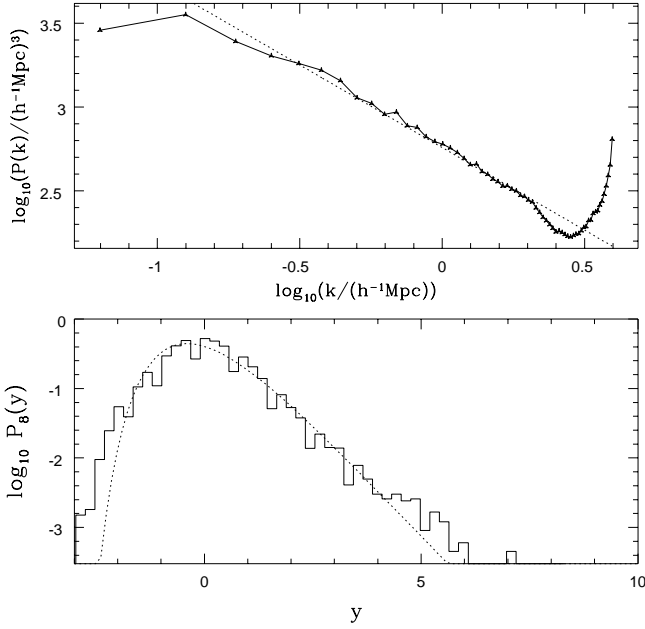


Figure 3. Measured (solid lines) and fitted (dotted lines) power spectra (top panel) and PDF (bottom panel) in the ICDM-2.0 model.

$M > M_{\text{NL}}$, where M_{NL} is the typical nonlinear mass satisfying $\delta_c/\sigma_{R(M_{\text{NL}})} = 1$. We show regions for which $M < M_{\text{NL}}$ in our figures by using dotted lines to continue the $N_{>M}$ curves.

A rough estimate of the type of errors we might expect in the PS prediction for the non-Gaussian mass function comes from consideration of the correction factor f (see equation 7). For Gaussian fluctuations, the choice $f = 2$ gives a good fit to the number abundance of clusters observed in N-body simulations, and is justified analytically by the excursion set derivation of the PS formula (Bond et al. 1991). For the non-Gaussian case, we have again fixed f by ensuring that the mass function accounts for the entire mass of the universe, thus maintaining the spirit of the PS derivation. However, we cannot be sure *a priori* that this correction will still account correctly for the number abundance of the rarest peaks. For the ICDM-2.4 model, the correction factor corresponding to the PDF used in our calculations is $f = 2.6$, suggesting that errors of order 30% in the predicted mass function would not be surprising.

We quantify the goodness of fit of the predictions at each redshift by computing the mean and the *rms* error, where the mean error \bar{E} is given by

$$\bar{E} = \frac{1}{j} \sum_{i=1}^j (N_{>M_i} - N_{>M_i}^S), \quad (31)$$

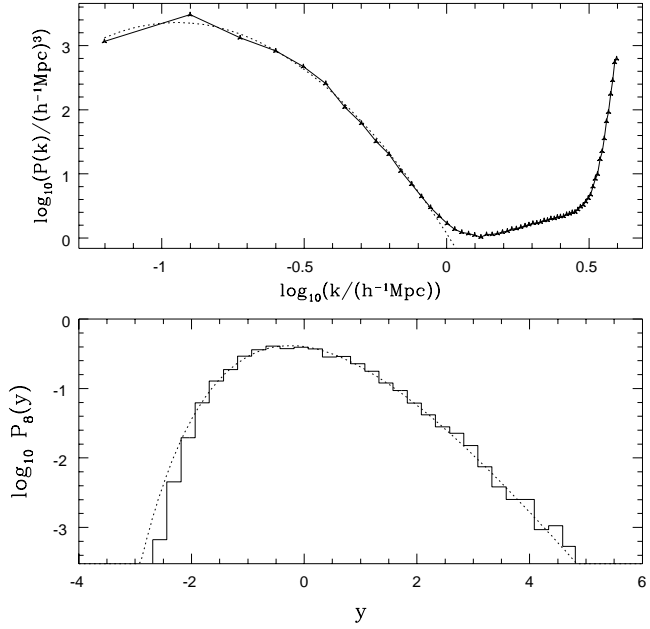


Figure 4. Measured (solid lines) and fitted (dotted lines) power spectra (top panel) and PDF (bottom panel) in the Strings-HDM model.

and the *rms* error $\sqrt{\bar{E}^2}$ is given by

$$\sqrt{\bar{E}^2} = \left(\frac{1}{j} \sum_{i=1}^j (N_{>M_i} - N_{>M_i}^S)^2 \right)^{1/2}. \quad (32)$$

Here M_i is the mass corresponding to the i^{th} data point and j is the number of data points. Together, these two measurements allow us to quantify both the systematic error in our predictions, as well as the scatter about them. Errors for each redshift are quoted in Table 2. In computing these errors we do not attempt to fit for points for which $M < M_{\text{NL}}$, since the PS formalism is known to break down for these masses in the Gaussian case. We see that typical errors are less than of order 0.1 in $\log_{10}(N_{>M}/(h^{-1}\text{Mpc})^3)$. The worst systematic error is for the Voids model at $z = 1.7$, where $\bar{E} = 0.11$. The worst *rms* error is for the Strings-HDM model at $z = 0$, where $\sqrt{\bar{E}^2} = 0.18$. Even in these worst cases, the errors are of order or smaller than typical measurement errors in $N_{>M}$, and many orders of magnitude smaller than the amount by which predictions for different models can differ.

6 CONCLUSIONS

We have carried out N-body simulations of a number of models with non-Gaussian initial conditions, and verified that a

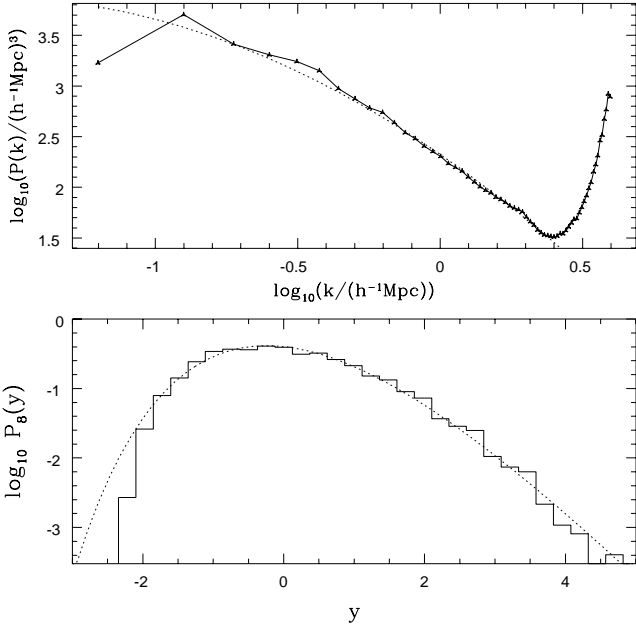


Figure 5. Measured (solid lines) and fitted (dotted lines) power spectra (top panel) and PDF (bottom panel) in the Strings-CDM model.

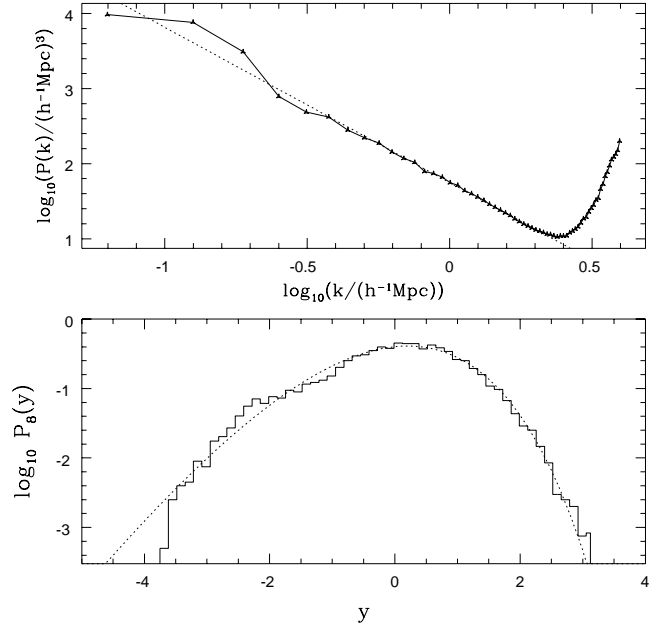


Figure 6. Measured (solid lines) and fitted (dotted lines) power spectra (top panel) and PDF (bottom panel) in the Voids model.

Model	z	\bar{E}	$\sqrt{\bar{E}^2}$
GA-1.8	0.0	0.006	0.044
	0.66	0.080	0.10
	1.5	-0.052	0.097
ICDM-2.4	0.0	0.10	0.12
	3.0	0.049	0.064
	5.7	-0.051	0.16
ICDM-2.0	0.0	0.14	0.90
	1.0	0.066	0.11
	2.0	-0.056	0.12
Strings-HDM	0.0	0.033	0.18
	0.33	-0.052	0.11
	1.0	-0.040	0.16
Strings-CDM	0.0	0.10	0.12
	1.0	0.081	0.10
	2.0	0.005	0.065
Voids	0.0	0.047	0.13
	1.0	0.057	0.084
	1.7	0.11	0.13

Table 2. Mean and *rms* errors in the predicted mass functions at each redshift.

modified version of the Press-Schechter formalism is able to give a good fit to the observed evolution of the cluster number abundance over a wide range of redshifts. While we have only tested the fit for a finite number of models, the models span a range of possible types of non-Gaussian behaviour. The ICDM and string models have a skew positive PDF, and typically give rise to more clusters of a given mass than would be expected in the corresponding Gaussian case. The Voids model has a skew negative PDF, and typically gives rise to fewer clusters than would be expected in the corresponding Gaussian case. The ICDM model is generated purely by a local transformation on a Gaussian field, so might be thought most likely to agree with the PS prediction. The Voids model, on the other hand, is generated by a more complex non-local transformation of a Gaussian random field, and the strings models are generated by an entirely different process altogether.

Quantitatively, the fits to the predicted mass function are slightly worse in the non-Gaussian models than in the Gaussian one. Typical fits in the non-Gaussian models have *rms* errors in $\log_{10}(N_{>M}/(h^{-1} \text{Mpc})^3)$ of $\sqrt{\bar{E}^2} \simeq 0.1$, corresponding to an error of roughly 25% in $N_{>M}$. The worst fit is in the $z = 0$ output of a strings model, where the *rms* error is $\sqrt{\bar{E}^2} = 0.18$, or roughly 50% in $N_{>M}$. These errors are of order or smaller than typical observational uncertainties in the determination of the mass function, and considerably

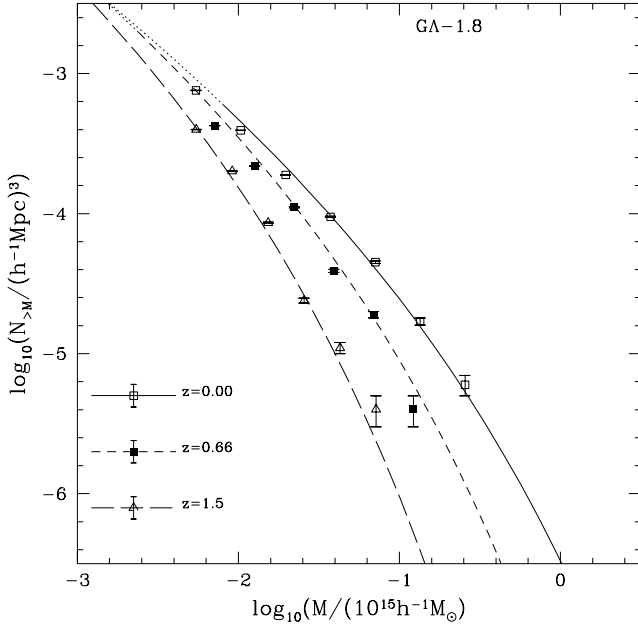


Figure 7. PS prediction for the mass function (curves) and that measured in simulations (data points) at various redshifts in the Gaussian GA-1.8 model.

smaller than the amount by which predictions for different models may differ.

Given uncertainties at this level, our results make it possible to use observations of cluster evolution to place strong constraints on non-Gaussianity in the primordial universe. The constraints from current cluster data are outlined in detail in Robinson et al. (in preparation). Given an independent measure of the matter density of the universe Ω_m (which we can hope to gain in the near future from the combination of supernovae and CMB observations), cluster evolution directly constrains the probability distribution function (PDF) of primordial fluctuations in the universe. If we assume $\Omega_m = 1$, Robinson et al. show that current data detects non-Gaussianity, and constrains the primordial PDF to have at least 2.5 times as many $3-\sigma$ peaks as a Gaussian distribution. If we assume $\Omega_m = 0.3$, current data is consistent with Gaussian fluctuations, with the PDF constrained to have no more than 9 times as many $3-\sigma$ peaks as a Gaussian distribution. Taken together with the substantial increase of data on high redshift clusters we can expect in the near future, the techniques described here can provide powerful, model independent constraints on non-Gaussianity in the primordial universe.

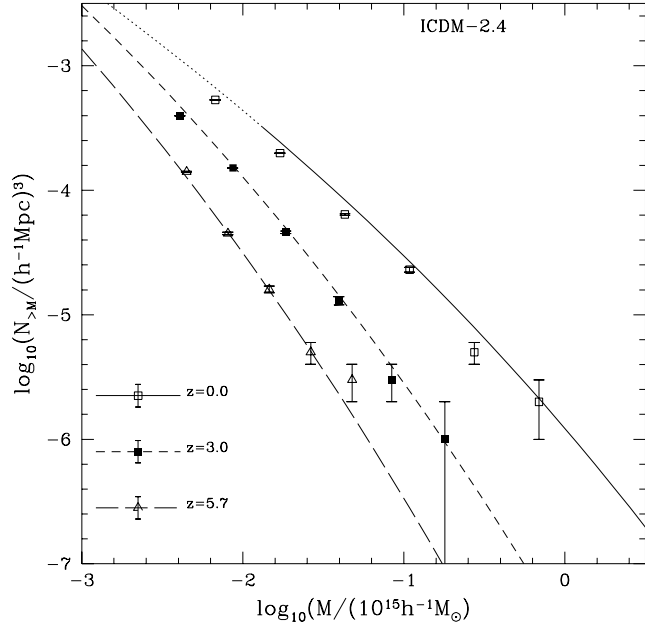


Figure 8. PS prediction for the mass function (curves) and that measured in simulations (data points) at various redshifts in the ICDM-2.4 model.

7 ACKNOWLEDGEMENTS

We would like to thank Marc Davis, Eric Gawiser, Joseph Silk, and Jochen Weller for helpful and stimulating discussions. We would also like to thank Pedro Ferreira for the use of his string evolution code. This work has been supported in part by grants from the NSF, including grant AST95-28340.

REFERENCES

- Albrecht A., Battye R. A., Robinson, J., 1997, PRL, 79, 4736
- Allen B., Caldwell R. R., Dodelson S., Knox L., Shellard E. P. S., Stebbins A., 1997, PRL, 79, 2624
- Amendola A., Borgani S., 1994, MNRAS, 266, 191
- Amendola A., Occhionero F., 1993, ApJ, 413, 39
- Avelino P. P., Shellard E. P. S., Wu J. H. P., Allen, B., 1998, PRL, 81, 2008
- Battye R. A., Robinson J., Albrecht A., 1998, PRL, 80, 4847
- Bond J. R., Cole S., Efstathiou G., Kaiser N., 1991, ApJ, 379, 440
- Borgani S., Coles P., Moscardini L., Manolis P., 1994, MNRAS, 266, 524
- Brieu P. P., Summers F. J., Ostriker J. P., 1995, ApJ, 453, 566
- Chiu W. A., Ostriker J. P., Strauss M. A., 1997, ApJ, 494, 479
- Ferreira P., 1995, PhD Thesis, Imperial College
- Kibble T. W. B., 1976, J. Phys., A9, 1387
- La D., 1991, PRB, 265, 232
- Lacey C., Cole S., 1993, MNRAS, 262 627

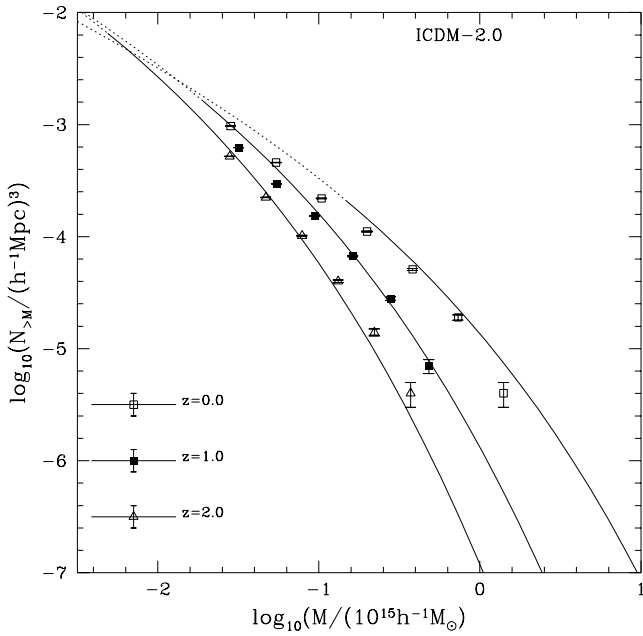


Figure 9. PS prediction for the mass function (curves) and that measured in simulations (data points) at various redshifts in the ICDM-2.0 model.

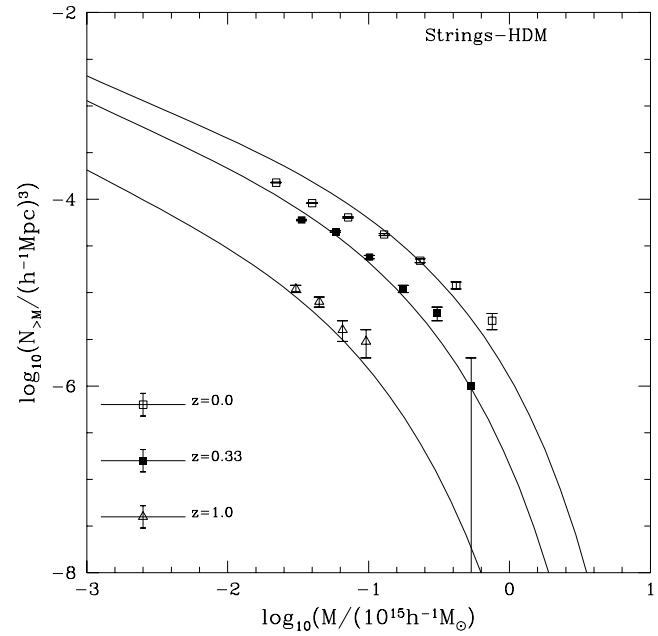


Figure 10. PS prediction for mass function (curves) and that measured in simulations (data points) at various redshifts in the Strings-HDM model.

Mo H. J., Jing Y. P., White S. D. M., 1996, MNRAS, 284, 189
 Park C., Spergel D. N., Turok N., 1991, ApJ, 372, L53
 Peebles P. J. E., 1983, ApJ, 274, 1
 Peebles P. J. E., 1997, ApJ, 483, L1
 Peebles P. J. E., 1998, astro-ph/9805194
 Peebles P. J. E., 1998, astro-ph/9805212
 Press W. H., Schechter P., 1974, ApJ, 187, 425
 Robinson J., Gawiser E., Sill J., 1998, astroph/9805181
 Smith A. G., Vilenkin A., 1987, PRD, 36, 990
 van de Bruck C., 1998, astroph/9810409
 Veeraraghavan S., Stebbins A., ApJ, 365, 37
 Vilenkin A., Shellard E. P. S., 1994, *Cosmic strings and other topological defects*. Cambridge Univ. Press, Cambridge
 Weinberg D. H., Cole S., 1992, MNRAS, 259, 652
 Zeldovich, Y. 1970, A&A, 5, 84

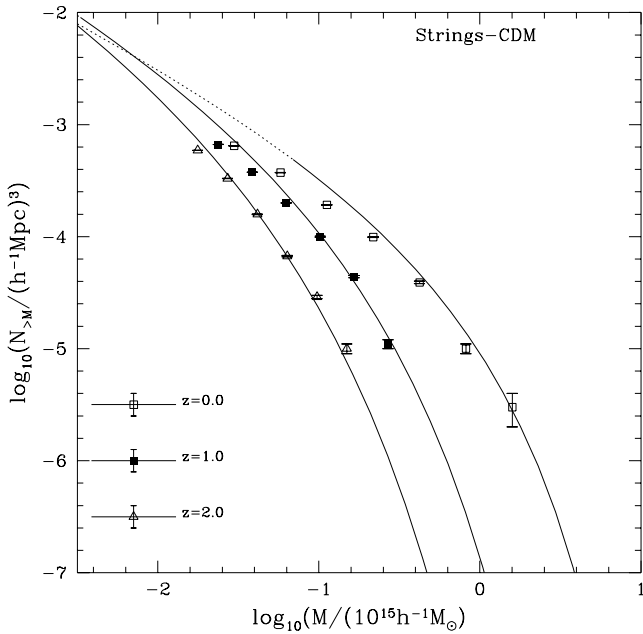


Figure 11. PS prediction for mass function (curves) and that measured in simulations (data points) at various redshifts in the Strings-CDM model.

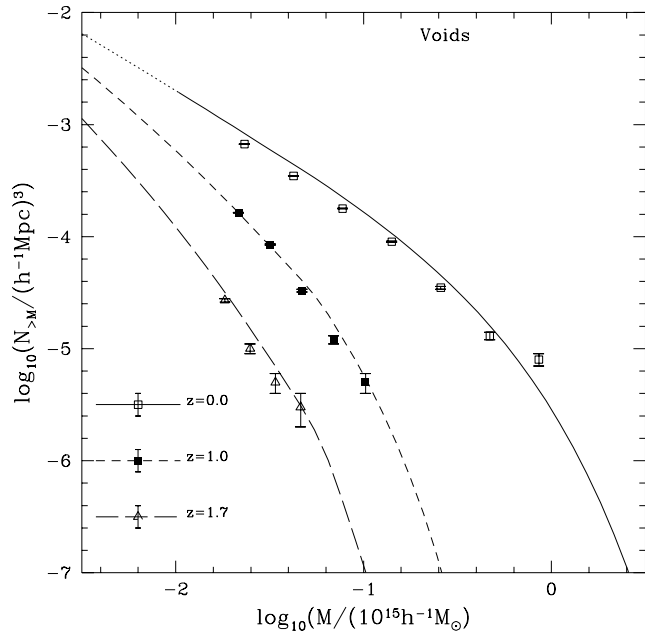


Figure 12. PS prediction for the mass function (curves) and that measured in simulations (data points) at various redshifts in the Voids model.